Neutron Reflectometry Elucidates Density Profiles of Deuterated Proteins Adsorbed onto Surfaces Displaying Poly(ethylene glycol) Brushes: Evidence for Primary Adsorption

ARTICLE *in* LANGMUIR · OCTOBER 2013

Impact Factor: 4.46 · DOI: 10.1021/la403355r · Source: PubMed

7 AUTHORS, INCLUDING:

Emanuel Schneck
Max Planck Institute of Colloids and Interfaces
42 PUBLICATIONS **297** CITATIONS
SEE PROFILE

Avraham Halperin
French National Centre for Scientific Research
119 PUBLICATIONS **3,906** CITATIONS
SEE PROFILE

Michael Haertlein
Institut Laue-Langevin
141 PUBLICATIONS **2,721** CITATIONS
SEE PROFILE

Giovanna Fragneto
Institut Laue-Langevin
140 PUBLICATIONS **2,612** CITATIONS
SEE PROFILE

Langmuir

Article

pubs.acs.org/Langmuir

Neutron Reflectometry Elucidates Density Profiles of Deuterated Proteins Adsorbed onto Surfaces Displaying Poly(ethylene glycol) Brushes: Evidence for Primary Adsorption

Emanuel Schneck,[†] Audrey Schollier,[†,‡] Avraham Halperin,[§] Martine Moulin,[†] Michael Haertlein,[†] Michele Sferrazza,[‡] and Giovanna Fragneto*[,†]

[†]Institut Laue-Langevin, 38042 Grenoble, France

[‡]Départment de Physique, Faculté des Sciences, Université Libre de Bruxelles, 1050 Brussels, Belgium

[§]Laboratoire Interdisciplinaire de Physique, Université Joseph Fourier Grenoble, CNRS UMR 5588, BP 87, 38042 Saint-Martin d'Hères, France

Supporting Information

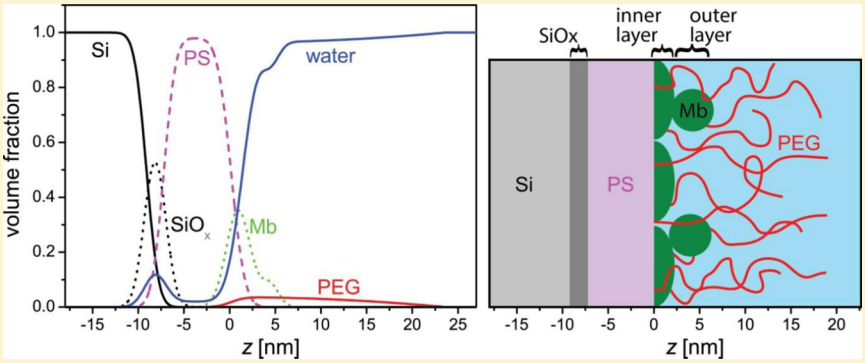

ABSTRACT: The concentration profile of deuterated myoglobin (Mb) adsorbed onto polystyrene substrates displaying poly(ethylene glycol) (PEG) brushes is characterized by neutron reflectometry (NR). The method allows to directly distinguish among primary adsorption at the grafting surface, ternary adsorption within the brush, and secondary adsorption at the brush outer edge. It complements depth-insensitive standard techniques, such as ellipsometry, radioactive labeling, and quartz crystal microbalance. The study explores the effect of the PEG polymerization degree, N, and the grafting density, σ, on Mb adsorption. In the studied systems there is no indication of secondary or ternary adsorption, but there is evidence of primary adsorption involving a dense inner layer at the polystyrene surface. For sparsely grafted brushes the primary adsorption involves an additional dilute outer protein layer on top of the inner layer. The amount of protein adsorbed in the inner layer is independent of N but varies with σ, while for the outer layer it is correlated to the amount of grafted PEG and is thus sensitive to both N and σ. The use of deuterated proteins enhances the sensitivity of NR and enables monitoring exchange between deuterated and hydrogenated species.

I. INTRODUCTION

The interactions between polymer brushes and nanoparticles are encountered and utilized in a wide variety of domains from materials science to biotechnology. Examples include the formulation of nanocomposites,[1] prolongation of the circulation time of protein drugs,[2] and harvesting of cell sheets for tissue engineering.[3] The interactions manifest themselves in the spatial distribution of the particles within the brush. This distribution can be determined experimentally by electron microscopy and X-ray reflectometry when inorganic particles such as gold nanocrystals are involved.[4] However, these techniques are inapplicable to biotechnology systems involving proteins interacting with water-swollen brushes of polymers such as poly(ethylene glycol) (PEG) and poly(*N*-isopropylacrylamide) (PNIPAM). The measurement methods typically implemented to characterize protein adsorption include radioactive labeling, quartz crystal microbalance (QCM), ellipsometry, and so forth.[5] These techniques yield the total amount adsorbed per unit area, Γ, but cannot resolve the concentration profile of the adsorbed proteins. Evidence on the concentration profiles has so far been obtained only indirectly, from the dependence of Γ on the grafting density,[6−9] that is, the number of polymers per surface area, σ. In the following we describe the use of neutron reflectometry (NR) to characterize the concentration profile of adsorbed proteins within PEG brushes differing in σ and polymerization degree N. The

Received: August 30, 2013
Revised: October 16, 2013
Published: October 21, 2013

sensitivity of the method is enhanced by the use of contrast variation and deuterated proteins. To our knowledge we obtain the first direct evidence for primary protein adsorption[10,11] at the surface anchoring the brush. For sparsely grafted brushes this primary adsorption involves two layers. Such "two layer" adsorption was recently reported for the same protein on bare surfaces.[12] For the particular protein we studied, myoglobin (Mb), there is no evidence of ternary adsorption[7−9] within the brush itself or of secondary adsorption[10,11,13] at the brush outer edge. Here, we investigate the effect of N and σ on the structure of the two protein layers. We also explore the potential of combining NR with deuterated proteins, thus enhancing the sensitivity of the technique and permitting its use to probe exchange of deuterated and hydrogenated species. The accessibility of this approach grows with the emergence of dedicated protein deuteration facilities (http://www.ill.eu/sites/deuteration/).

Our results concerning the concentration profiles of adsorbed proteins within brushes are of interest from two points of view. From a fundamental perspective they contribute to the understanding of protein adsorption mechanisms and enable confrontation with theoretical models on the topic.[6] The results are also of practical interest in guiding rational brush design for biotechnology applications. Two systems illustrate the last point: first, brushes of PEG utilized to repress protein adsorption[14−16] as deployed in the pharmaceutical industry to prolong the circulation time of protein drugs, stealth liposomes, and so forth;[3] and second, thermoresponsive tissue culture substrates based on PNIPAM brushes as utilized to harvest confluent cell sheets for tissue engineering.[17−19] The protein adsorption modes affect the design and performance of both PEG[6,8,9] and PNIPAM[20−23] brushes. The use of NR to resolve the concentration profile of proteins adsorbed within brushes may provide additional insights concerning the biocompatibility of surfaces displaying polymer brushes.

II. EXPERIMENTAL SECTION

A. Sample Preparation. Sample preparation started from silicon single (111) crystals of 80 mm × 50 mm × 10 mm size, covered with a thin amorphous silicon oxide (SiO_x) layer at the surface, and cleaned by washing with organic solvents (chloroform, acetone, and ethanol) and UV-ozone treatment.[24] The brushes were deposited onto the silicon substrates in a previously reported three-step procedure.[7,25−27] First, a layer of vinyl-terminated polystyrene (PS), of weight-averaged molecular mass M_W = 2100 Da, was deposited onto the silicon surfaces from 1 mg/mL chloroform solutions. The polydispersity of the PS was M_W/M_n = 1.11, where M_n denotes the number-averaged molecular mass. Residual chloroform was evaporated with a stream of nitrogen,[25,26] and the silicon blocks were then heated to 150 °C under vacuum to allow the vinyl-ends to form covalent bonds with the SiO_x surface.[7,25−27] This first PS layer promotes wetting by a second PS layer, deposited by spin-coating a 1 mg/mL solution of PS (M_W = 1050 kDa, M_W/M_n = 1.19) in toluene. The resulting PS layer was stable and homogeneous, with a thickness of about 6 nm as measured by ellipsometry. PEG brushes were deposited onto the PS surface utilizing the Langmuir−Schaefer (LS) technique,[28] from a 1 mg/mL chloroform solution of PS-PEG diblock copolymers (Polymer Source Inc., Canada) with short PS (N_{PS} = 37, M_W = 3990 Da) and longer PEG blocks (N = 146, M_w = 6424 Da and N = 770, M_w = 33 880 Da). Monolayers were prepared by spreading the chloroform solution at the air−water interface in a Teflon Langmuir trough (Nima Technology, Coventry, UK) containing ultrapure water. After compression of the PS-PEG monolayer to defined lateral densities and subsequent deposition onto the PS surface, the wafers were heated to 100 °C. This promotes the diffusion of the PS blocks of the PS-PEG diblock copolymers into the PS sublayer, leading to effectively irreversible attachment of the PEG brush to the surface.[7,25−27] The resulting grafting densities σ were determined by NR.

Deuterated myoglobin (Mb) of molecular weight 20.6 kDa was expressed and purified at the ILL Deuteration Laboratory using a procedure described earlier.[29] In essence, the recombinant protein was produced in high cell density cultures with fully deuterated minimal medium and fully deuterated glycerol as a carbon source.[30,31] The crystallographic structure of fully deuterated Mb as obtained by neutron diffraction is similar to that of the hydrogenated Mb.[32] A single Mb is a globular protein with dimensions of about 45 Å × 35 Å × 25 Å and an effective equivalent radius $r_{Mb} \approx 20$ Å.[33] It is known to be a "soft" protein; that is, it undergoes conformational changes upon adsorption at solid−liquid interfaces as observed by circular dichroism and infrared spectroscopy.[34,35] The neutron scattering length density (SLD) of Mb, ρ_{Mb}, depends on the D_2O/H_2O ratio of its aqueous environment because of the dynamic exchange of labile hydrogens with the solvent. The amino acid sequence of the recombinant Mb identifies a total of 1381 hydrogens. Among them 303 (22%) are bound to nitrogen, oxygen, or sulfur atoms and are thus considered labile and subject to exchange with hydrogen atoms of water. This estimate is in good agreement with mass spectroscopy measurements demonstrating 21% of exchange[12] and earlier results.[32] After characterization of the bare polymer brushes by NR, the samples were immersed for 12 h in a 0.8 mg/mL solution of deuterated Mb in H_2O, then rinsed, and finally characterized by NR sequentially in various water contrasts.

B. Neutron Reflectometry and Data Analysis. Neutron reflectometry (NR) measurements were performed on the D17 neutron reflectometer at the Institut Laue-Langevin (Grenoble, France).[36] The intensity of the reflected neutron beam relative to the intensity of the incident beam was recorded as a function of $q_z = (4\pi/\lambda) \sin \theta_i$, the component of the scattering vector normal to the interface, where λ is the neutron wavelength and θ_i the incident angle. Measurements were carried out in time-of-flight (TOF) mode with a wavelength range of 2 Å < λ < 20 Å at two fixed angles of incidence, θ_i = 0.70° and θ_i = 3.00°, thus covering a q_z-range of 0.008 Å^{-1} < q_z < 0.25 Å^{-1}. In our experiment, the relative resolution in q_z, $\Delta q_z/q_z$, was q_z-dependent and varied in the range 1% < $\Delta q_z/q_z$ < 10%. While modeling experimental reflectivity curves, the finite experimental resolution was taken into account by convoluting the initial reflectivity curves, calculated for the case of infinite resolution, with Gaussian functions representing the resolution function of the experiments. The reflectivity curves displaying the reflected intensity as a function of q_z depend on the depth profile of the neutron scattering length density:

$$\rho(z) = \sum_i n_i(z) b_i \tag{1}$$

where $n_i(z)$ and b_i denote respectively the number density at altitude z and the coherent scattering length of nuclide i. Due to the large difference between the scattering lengths of hydrogen, b_H, and deuterium, b_D, contrast variation can be used to highlight the scattering contributions from the various components of an interface. The ambiguity of a model fit is strongly reduced by characterizing the same sample in different "water contrasts", that is, in aqueous subphases of different H_2O/D_2O ratios and thus of different SLD, ρ_w. In this work we utilized up to four contrasts per sample: pure D_2O ($\rho_w = 6.36 \times 10^{-6}$ Å^{-2}), pure H_2O ($\rho_w = -0.56 \times 10^{-6}$ Å^{-2}), as well as mixtures with SLDs of $\rho_w \approx 4.0 \times 10^{-6}$ Å^{-2} (often termed *4-matched water*) and $\rho_w \approx 2.1 \times 10^{-6}$ Å^{-2} (often termed *silicon matched water*). Deviations in the scattering length density of water, introduced by the incompleteness of the liquid exchange in the measurement cells, were accounted for by adjusting the corresponding ρ_w parameters during the fitting procedure, noting that the addition of each adjustable parameter leads to a slight increase in the errors bars. [The incomplete mixing of D_2O and H_2O is caused by the different densities of the two liquids and the vertical geometry of the sample cell on the reflectometer. In the used cell design solvent replacement is done in situ with an injection port at the bottom of the cell and the exit port positioned on the top. This problem has been recently identified and improved cells are currently being designed. Nevertheless, the SLD

parameter corresponding to the water contrast can be fitted for each curve. The obtained values are reported in Table S1 of the Supporting Information.]

The reflectivity data were analyzed as follows: each sample, identified by N and σ, was described by a common model allowing for all measurement conditions, that is, the different water contrasts before and after incubation with Mb. The model describes the volume fractions Φ of all compounds, that is, silicon (Si), silicon oxide (SiO_x), PS, PEG, Mb, and water (w), and incorporates a number of adjustable parameters that are fitted simultaneously to the results obtained in different conditions. For each measurement the corresponding SLD density profile is given by:

$$\rho(z) = \Phi_{Si}(z)\rho_{Si} + \Phi_{SiO_x}(z)\rho_{SiO_x} + \Phi_{PS}(z)\rho_{PS} + \Phi_{PEG}(z)\rho_{PEG} + \Phi_{Mb}(z)\rho_{Mb} + \Phi_{w}(z)\rho_{w} \quad (2)$$

where z denotes the distance measured perpendicular to the planar sample surface. The brush grafting surface is at $z = 0$, and the aqueous phase occupied the $z > 0$ range. Equations 1 and 2 are equivalent representations of the SLD profile. In the following we use eq 2 because our interest concerns components, proteins, and PEG, rather than the constituting nuclides. The treatment of the $z < 0$ range, comprising Si, SiO_x, and PS regions, is straightforward. The crystalline silicon substrate is modeled by a semi-infinite continuum with scattering length density $\rho_{Si} = 2.07 \times 10^{-6}$ Å^{-2}. The SiO_x and PS layers are depicted as two homogeneous slabs with adjustable thicknesses (d_{SiO_x} and d_{PS}), dry SLDs (ρ_{SiO_x} and ρ_{PS}), and water contents ($\Phi_w^{SiO_x}$ and Φ_w^{PS}). To account for the interfacial roughness, the concentration profiles of the slabs are modulated by error functions with adjustable roughness parameters ζ. The key ingredient for our analysis is the description of the $z > 0$ range reflecting the contributions of the PEG brush, $\Phi_{PEG}(z)$, the adsorbed Mb, $\Phi_{Mb}(z)$, and the solvent, $\Phi_w(z)$, such that $\Phi_{PEG}(z) + \Phi_{Mb}(z) + \Phi_w(z) = 1$. In the following we will discuss $\Phi_{PEG}(z)$ and $\Phi_{Mb}(z)$ at length. We first note that ρ_{PEG} and ρ_{Mb} are the dry SLDs of PEG and Mb, respectively. The values of ρ_w and ρ_{Mb} are different for each water contrast. Assuming that the H/D ratio of the labile hydrogen atoms in Mb is set by the isotopic composition of the aqueous medium we obtain $\rho_{Mb} = 6.75 \times 10^{-6}$ Å^{-2}, $\rho_{Mb} = 7.21 \times 10^{-6}$ Å^{-2}, and $\rho_{Mb} = 7.55 \times 10^{-6}$ Å^{-2} in H_2O, *silicon-matched water*, and *4-matched water*, respectively. ρ_{PEG} is independent of the H_2O/D_2O ratio and set equal to the recently determined value 0.6×10^{-6} Å^{-2} [37].

We model the PEG brush contribution by using

$$\Phi_{PEG}(z) = I(z)\Phi_P(z) \quad (3)$$

where

$$I(z) = \frac{1}{2}\left[1 + \mathrm{erf}\left(\frac{z}{\sqrt{2\zeta_{PS}^2}}\right)\right] \quad (4)$$

allows for the topographical roughness ζ_{PS} of the sharp PS/water interface utilizing the error function erf(x) and

$$\Phi_P(z) = \Phi_0\left(1 - \frac{z^2}{H_0^2}\right) \qquad 0 \le z \le H_0 \quad (5)$$

describes the concentration profile of a brush anchored to a planar surface and characterized by its maximal height H_0 and maximal PEG volume fraction Φ_0. The $I(z)$ factor affects $\Phi_{PEG}(z)$ in the immediate vicinity of the grafting surface at $z = 0$. It gives rise to an effective depletion region as well as to weak penetration of the brush into the PS region (Figure 3b). With regard to $\Phi_P(z)$ it is important to first note that the data can be fitted by a variety of functional forms such as a step function, suggested by the Alexander model,[38] and by a purely empirical stretched exponential. The reflectivity curves do not exhibit minima in the low-q_z range, thus indicating a gradually decreasing concentration profile. This, together with the results of self-consistent field (SCF) theory,[39−41] motivates our choice of $\Phi_P(z)$ (eq 5). While the parabolic profile is motivated by the SCF theory, it is important to note two caveats. First, in the SCF theory Φ_0 and H_0 are "brush constants" determined by N, σ, and T such that for a marginal solvent $\Phi_0 H_0 = 3a^3N\sigma/2$, where a is the monomer size. In contrast, Φ_0 and H_0 in $\Phi_{PEG}(z)$ are independent fitting parameters. Second, the SCF theory applies to strongly interpenetrating chains of high N such that $\sigma \gg R_F^{-2}$, where $R_F = aN^{3/5}$ is the Flory radius of the chain. We however utilize $\Phi_{PEG}(z)$ for all samples including cases with $\sigma \gtrsim R_F^{-2}$. The estimate of the overlap threshold depends on the value of a. The a values cited in the literature vary between 3.3 Å and 4.4 Å.[42,43] The Kuhn length and the related number p of monomers in a persistent length also affect the overlap threshold. Estimates for p vary in the range $1 < p \le 3$.[42,44,45] In the following we utilize $a = 4.1$ Å as determined from ρ_{PEG} via $\rho_{PEG} = b_{PEG}/a^3$, where b_{PEG} is the total scattering length of a PEG monomer. To this end we use the recent value $\rho_{PEG} = 0.6 \times 10^{-6}$ Å^{-2},[37] noting that a slightly higher value, $\rho_{PEG} = 0.64 \times 10^{-6}$ Å^{-2} was reported earlier.[46]

Our model of the Mb concentration profiles is chosen so as to allow for the different protein adsorption modes recognized in the literature: primary adsorption at the grafting surface, ternary adsorption within the brush, and secondary adsorption at the outer edge of the brush. To this end we consider inner and outer Mb sublayers such that the overall Mb contribution is

$$\Phi_{Mb}(z) = \Phi_{Mb}^{in}(z) + \Phi_{Mb}^{out}(z) \quad (6)$$

The primary adsorption scenario is taken into account via an inner layer, $\Phi_{Mb}^{in}(z)$, of thickness d_{in} at the grafting surface. Apart from roughness corrections, it is a homogeneous slab of constant protein volume fraction Φ_{in}. The roughness at the inner boundary, ζ_{PS}, reflects the topography of the sharp PS surface. Its outer boundary is characterized by ζ_{in} leading altogether to

$$\Phi_{Mb}^{in}(z) = \frac{\Phi_{in}}{2}\left[\mathrm{erf}\left(\frac{z}{\sqrt{2\zeta_{PS}^2}}\right) - \mathrm{erf}\left(\frac{z - d_{in}}{\sqrt{2\zeta_{in}^2}}\right)\right] \quad (7)$$

The outer Mb layer

$$\Phi_{Mb}^{out}(z) = \frac{\Phi_{out}}{2}\left[1 + \mathrm{erf}\left(\frac{z - d_{in}}{\sqrt{2\zeta_{in}^2}}\right)\right] \times \exp\left(-\frac{(z - z_{out})^2}{2\Delta z^2}\right) \quad (8)$$

was introduced with ternary and secondary adsorption in mind. The concentration profile is assumed to be Gaussian of amplitude Φ_{out} and width Δz centered at z_{out}. The Gaussian is truncated at the boundary of the inner layer. As we shall see, the chosen model leads to a satisfactory description of the experimental data. The precise choice of $\Phi_{Mb}^{in}(z)$ and $\Phi_{Mb}^{out}(z)$ is somewhat arbitrary. Alternative descriptions, invoking for instance two homogeneous layers,[12] involve the same number of adjustable parameters. Within the experimental errors they would lead to identical conclusions. To reduce the number of adjustable parameters in the simultaneous fits, we assume that the brush profiles are not modified by the protein adsorption. This assumption is strictly justified for sparsely adsorbed proteins of dimensions small enough to allow circumvention by the chain trajectories.[47] While these conditions are not met in all systems, introducing this assumption has negligible effect on the fits. This is because the reflectivity of protein-free samples is sensitive to the PEG brushes, while the proteins dominate the NR results when adsorption takes place.

To simultaneously fit the parameters of the common model to a set of experimental reflectivity curves, we utilized the following procedure. The initial value for the dry SLD of SiO_x was set to the literature value for silicon dioxide, $\rho_{SiO_2} = 3.4 \times 10^{-6}$ Å^{-2}. The dry SLD of the PS layer was initially set to the value reported earlier, $\rho_{PS} = 1.4 \times 10^{-6}$ Å^{-2}.[12] Initial values of d_{SiO_x} and d_{PS} were obtained from ellipsometry. The SLDs of H_2O/D_2O mixtures were initially set at the theoretical values corresponding to complete liquid exchange. Solvent fractions $\Phi_w^{SiO_x}$ and Φ_w^{PS} were initially set to 0. All roughness parameters had initial values of 5 Å. The initial values of the brush grafting density σ were

dx.doi.org/10.1021/la403355r | Langmuir 2013, 29, 14178−14187

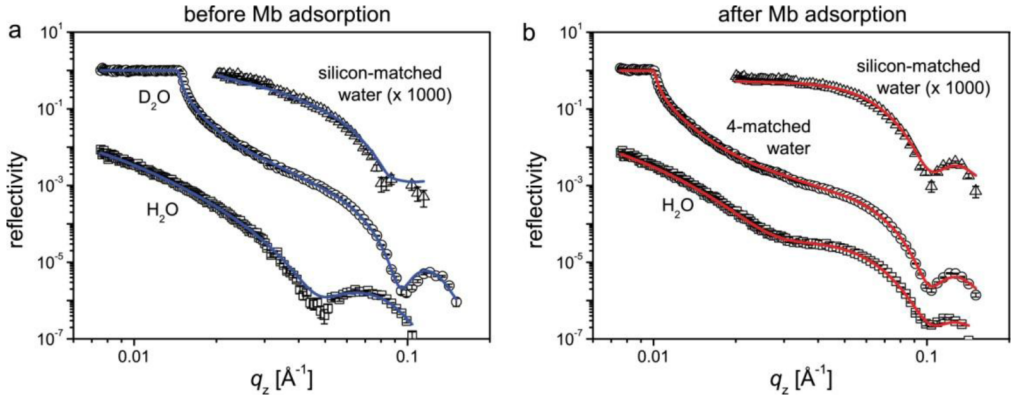

Figure 1. Representative set of reflectivity measurements (points) of a PEG brush (N = 770) in various water contrasts before (a) and after (b) adsorption of deuterated Mb. Solid lines depict the results of the best common model.

obtained from the area per PS-PEG diblock copolymer during LS transfer. For the other parameters (Φ_0, H_0, Φ_{in}, d_{in}, Φ_{out}, z_{out}, and Δz, see eqs 5, 7, and 8) several initial values spanning a wide parameter range were tested demonstrating that the fits are independent of the choice of the initial value. With these values at hand we first used eq 2 to calculate for each sample a set of interfacial SLD profiles $\rho(z)$ representing each water contrast before and after protein adsorption. In the next step we calculated the reflectivity curves corresponding to the $\rho(z)$ profiles using dynamical reflection theory. To this end the profiles were discretized into hundreds of thin slabs of 1 Å thickness of constant SLD. The q_z-dependent intensities were then calculated via application of Fresnel's reflection laws at each slab/slab interface using the iterative recipe of Parratt.[48] The reduced chi-square deviation χ^2_{red} between calculated and experimental sets of reflectivity curves was determined, and the best parameter set, with minimal χ^2_{red}, was found iteratively using Powell's method.[49] Error estimates were derived from the diagonal elements of the corresponding parameter covariance matrix.[50] During minimization, parameters were allowed to vary without restrictions. In the error estimation the parameter of interest is systematically displaced from its optimal value. During this process the brush extension H_0 occasionally had to be constrained to ensure $H_0 < Na$. Error bars for the total amount of protein in the inner layer were estimated for $\Phi^{out}_{Mb}(z)$ with constant z_{out} and Δz but allowing for variation in the amplitude Φ_{out}. Error bars for the total amount of protein in the outer layer were estimated from the difference between χ^2_{red} obtained for the two-layer model and for the one-layer model ($\Phi^{out}_{Mb}(z) \equiv 0$), while assuming parabolic form for the deviation of χ^2_{red} from its optimal value.

A typical set of data and the corresponding outcome of the analysis are depicted in Figures 1 and 2. As we shall elaborate later, the comparatively extended brush profiles manifest themselves in the low-q_z regime. On the other hand, the proteins adsorb as dense thin layers characterized by the position and the shape of the reflectivity minima at higher q_z. The bare brush was characterized in D_2O, silicon-matched water, and H_2O. After incubation it was characterized in silicon-matched water and H_2O and in the case shown in Figure 1 also in 4-matched water. Note that silicon-matched water data were analyzed only for $q_z > 0.02$ Å^{-1}, since this contrast is prone to background artifacts[51] at low q_z. The solid lines in Figure 1 correspond to the best common model obtained by the simultaneous fit of all curves. The global agreement is good considering that a single model is fitted simultaneously to six data sets. The corresponding reconstruction of the structure of the solid–liquid interface is depicted in Figure 2. The volume fractions Φ of all compounds are plotted as functions of z, illustrating the detailed structural information obtained from neutron reflectometry. We emphasize that the interpenetration of different compounds can reflect diffuse interfaces or topographical roughness of sharp interfaces. On physical grounds we consider the PS/water interface sharp and rough.

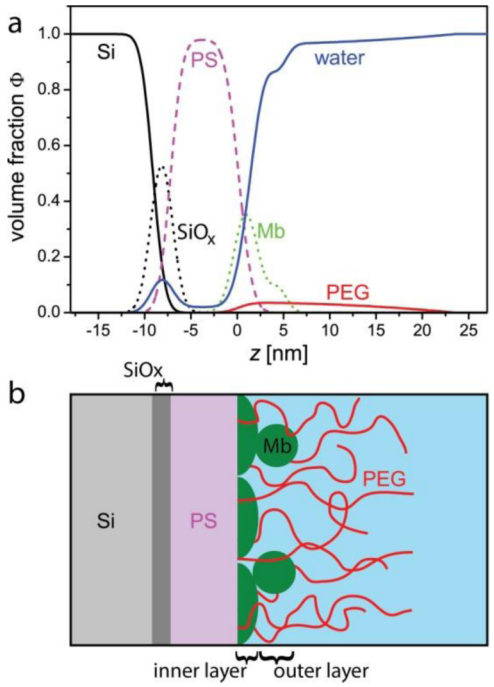

Figure 2. (a) Best-matching common model of the structure of the surface grafted PEG brush after Mb adsorption corresponding to the reflectivity curves presented in Figure 1. Volume fractions Φ of silicon (Si), silicon oxide (SiO_x), PS, PEG, Mb, and water are plotted as functions of the distance z perpendicular to the sample plane. z = 0 coincides with the grafting surface. (b) The interpretation of the concentration profiles, as discussed in the text, involves two sublayers of adsorbed Mb, a dense inner layer (depicted as hemiellipsoids) and a dilute outer layer (depicted as spheres).

III. RESULTS AND DISCUSSION

The principal results of our work concern the adsorption of Mb: the mass adsorbed per unit area, Γ_{Mb}, the corresponding Mb concentration profiles, and their dependence on the brush structure as characterized by N and σ. In the notation of the model all of the relevant information concerns the $z > 0$ region. Yet, it is important to comment on the NR results concerning the substrate comprising Si, SiO_x, and PS layers, in the $z < 0$ region. This is because this information provides a measure of the overall validity of the common model and because the roughness of the PS/water interface plays a role in modeling the brush and the adsorbed Mb layer. In the studied samples

dx.doi.org/10.1021/la403355r | Langmuir 2013, 29, 14178–14187

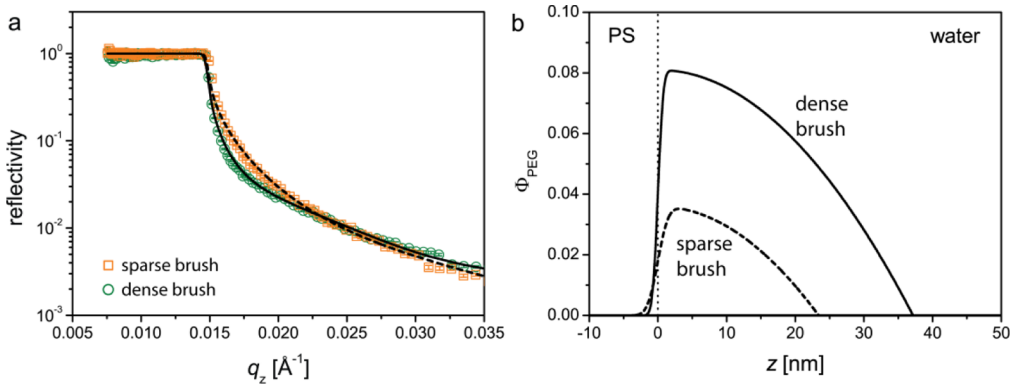

Figure 3. (a) Comparison between D_2O reflectivity data (symbols) of sparse ($\sigma = 1.1 \pm 0.8 \times 10^{16}$ m^{-2}) and dense ($\sigma = 5.2 \pm 0.9 \times 10^{16}$ m^{-2}) PEG $N = 770$ brushes. The lines represent the best-matching models. (b) The PEG monomer volume fraction $\Phi_{PEG}(z)$ corresponding to the best-matching models highlighting the differences between the SCF parabolic profile and $\Phi_{PEG}(z)$ as specified by eqs 3−5. Note in particular the "depletion" region in the vicinity of the grafting surface and the finite $\Phi_{PEG}(z)$ at $z < 0$. The sparse brush $\Phi_{PEG}(z)$ fit is not unique because of the large error bars associated with Φ_0 and H_0 (Table 1).

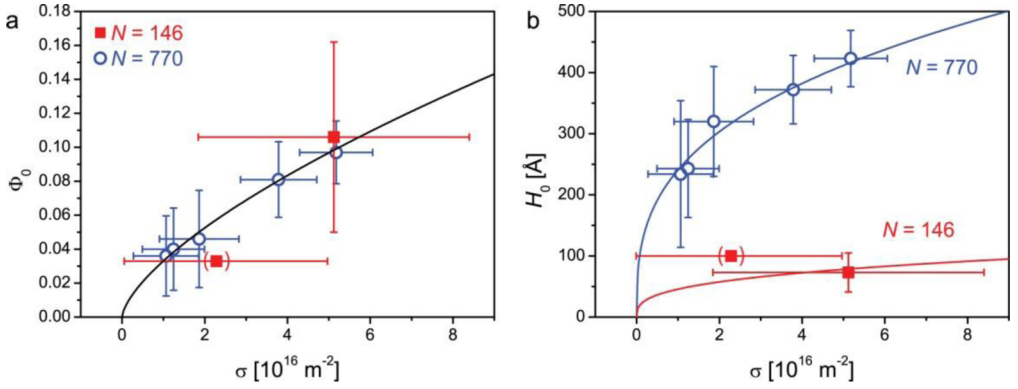

Figure 4. Brush parameters Φ_0 (a) and H_0 (b) for $N = 770$ (circles) and $N = 146$ (squares) as functions of the PEG grafting density σ together with $\Phi_0^{SCF}(\sigma)$ and $H_0^{SCF}(\sigma,N)$ for $p\tau = 0.33$ (solid lines). Vertical error bars of data points in brackets could not be determined.

Table 1. Characteristics of the PEG Brushes and of Mb Adsorption As Obtained by NR for the Samples Studied[a]

N	σ (10^{16} m^{-2})	Γ_{PEG} (mg m^{-2})	Φ_0	H_0 (Å)	Γ_{Mb} (mg m^{-2})	Γ_{Mb}^{in} (mg m^{-2})	Γ_{Mb}^{out} (mg m^{-2})
770	1.1 ± 0.8	0.6 ± 0.4	0.04 ± 0.02	(2.3 ± 1.2) × 10^2	1.8 ± 0.4	1.6 ± 0.3	0.3 (<0.5)
770	1.2 ± 0.8	0.7 ± 0.4	0.04 ± 0.02	(2.4 ± 0.8) × 10^2	1.9 ± 0.4	1.8 ± 0.2	0.1 (<0.2)
770	1.9 ± 1.0	1.0 ± 0.5	0.05 ± 0.03	(3.2 ± 0.9) × 10^2	1.3 ± 0.5	1.3 ± 0.1	
770	3.8 ± 0.9	2.1 ± 0.5	0.08 ± 0.02	(3.7 ± 0.6) × 10^2	1.1 ± 0.5	1.1 ± 0.1	
770	5.2 ± 0.9	2.9 ± 0.5	0.10 ± 0.02	(4.2 ± 0.5) × 10^2	1.0 ± 0.5	1.0 ± 0.1	
146	2 (<5)	0.2 (<0.5)	[0.03]	[1.0 × 10^2]	2.2 ± 0.3	1.4 ± 0.1	0.8 ± 0.3
146	5 ± 3	0.6 ± 0.4	0.11 ± 0.06	(0.7 ± 0.3) × 10^2	1.4 ± 0.3	1.1 ± 0.2	0.3 ± 0.2

[a]For numbers in square brackets the associated error could not be determined. The overlap thresholds $\sigma = R_F^{-2}$ are $\sigma = 0.2 \times 10^{16}$ m^{-2} for $N = 770$ and $\sigma = 1.5 \times 10^{16}$ m^{-2} for $N = 146$, when $a = 4.1$ Å and $p = 1$.

the thickness of the SiO_x layer varied in the range $d_{SiO_x} = 17 \pm 5$ Å, with dry SLD $\rho_{SiO_x} = 3.5 \pm 0.9 \times 10^{-6}$ Å^{-2}, and water content $\Phi_w^{SiO_x} = 16 \pm 4$ vol %, in agreement with earlier reports in the literature.[52−54] The surface of the oxide layer is smooth and exhibits roughness $\zeta_{SiO_x} \leq 7$ Å. We attribute the variability of the oxide structural profile to the manufacturing history of individual silicon blocks and to the effects of heat treatment involving temperatures of up to 150 °C.[55] The structure of the PS layer exhibits weaker variation, with a thickness of $d_{PS} = 80 \pm 10$ Å, a negligible water content of $\Phi_w^{PS} < 4$ vol %, and a dry SLD of $\rho_{PS} = 1.34 \pm 0.09 \times 10^{-6}$ Å^{-2}, consistent with the literature value $\rho_{PS} = 1.40 \times 10^{-6}$ Å^{-2}.[12] Here we recall that our fitting procedure does not constrain the water contents and it does not allow for possible contributions due to residual solvents from the sample preparation. Note that within the detection limits the PS contains no water. In any case, the variations noted above have no significant impact on our results concerning the aqueous $z > 0$ region. The roughness of the PS/water interface, $\xi_{PS} = 10 \pm 4$ Å, plays a role in modeling PEG and Mb profiles.

A. Structure of the Surface-Grafted PEG Brushes. As noted earlier, the reflectivity of the bare PEG brushes before protein adsorption can be fitted with different $\Phi_{PEG}(z)$ functions. Importantly, σ and the PEG mass per surface area, Γ_{PEG}, are insensitive to the functional form, since they are specified by

dx.doi.org/10.1021/la403355r | Langmuir 2013, 29, 14178−14187

$$\Gamma_{PEG} = m_{PEG} N\sigma = \frac{m_{PEG}}{v_{PEG}} \int \Phi_{PEG}(z)\, dz \tag{9}$$

where m_{PEG} and $v_{PEG} = a^3$ are, respectively, the mass and the volume of a PEG monomer. The model independence follows from the required normalization condition, namely

$$\int \Phi_{PEG}(z)\, dz = Na^3\sigma \tag{10}$$

The parabolic brush profiles reproduce the bare-brush reflectivity curves as illustrated in Figure 3a. The brush signatures are clearly manifested in the differences between sparse and dense brushes in the low-q_z range. The best-matching brush profiles $\Phi_{PEG}(z)$ corresponding to the reflectivity curves in Figure 3a are characterized by the brush parameters Φ_0 and H_0 shown in Figure 3b (see also eqs 3–5). The fitted parameters Φ_0 and H_0 as functions of σ are depicted in Figure 4 and summarized in Table 1. Note that for the sparser $N = 146$ brush the obtained grafting density does not exceed the associated experimental error. We however report on this data point since the observed adsorbed protein amount is lower than for a bare PS substrate, indicating the presence of a sparse brush.

Our choice of the parabolic $\Phi_P(z)$ factor in $\Phi_{PEG}(z)$ was suggested by SCF results, where $\Phi_0^{SCF}(\sigma)$ and $H_0^{SCF}(\sigma,N)$ are specified by

$$\phi_0^{SCF}(\sigma) = \frac{3}{2}\left(\frac{\pi^2}{8p\tau}\right)^{1/3} (a^2\sigma)^{2/3} \tag{11}$$

$$H_0^{SCF}(\sigma, N) = \left(\frac{8p\tau}{\pi^2}\right)^{1/3} aN(a^2\sigma)^{1/3} \tag{12}$$

Here τ is a reduced temperature defined for polymers described by the Flory free energy and p the number of monomers in a persistent segment. In contrast to Φ_0 and H_0 in eq 5, $\Phi_0^{SCF}(\sigma)$ and $H_0^{SCF}(\sigma,N)$ are not free variables. Interestingly, $\Phi_0^{SCF}(\sigma)$ and $H_0^{SCF}(\sigma,N)$ reproduce the experimentally obtained Φ_0 and H_0 upon adjustment of $p\tau$. For $a = 4.1$ Å, set by the SLD of PEG, the best agreement is obtained for $p\tau = 0.33$. It is important to note that when applied to PEG τ is an unspecified dimensionless function of T rather than the familiar $\tau = 1 - \Theta/T$ defined in terms of the Θ temperature.[8] Note also that the applicability of the SCF theory (eqs 11 and 12) to polymers exhibiting a lower critical solution temperature (LCST) such as PEG remains to be discussed.

B. Density Profiles of Adsorbed Mb. The reflectivity of all samples, irrespective of σ and N, changes significantly upon incubation in solutions of deuterated Mb, indicating significant protein adsorption at the solid/liquid interface (Figure 5). The curves after Mb adsorption exhibit distinct changes in the q_z positions of the minima, associated with the formation of dense protein layers. This conclusion is independent of the brush model. In all cases the parameters of the common model reveal that protein adsorption occurs at the PS surface. There is no indication of secondary adsorption at the outer edge of the brush or ternary adsorption within the brush. Here we note that the functional form of the common model allows for the possibility of secondary or ternary adsorption (see Experimental section). The results of the fitting procedure thus rule out scenarios of significant secondary or ternary protein adsorption.

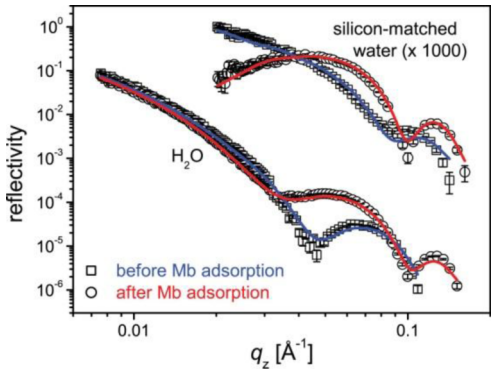

Figure 5. Comparison between reflectivity measurements of a surface-grafted polymer brush with $N = 770$ and $\sigma = 5.2 \pm 0.9 \times 10^{16}$ m^{-2} before and after Mb adsorption in silicon-matched water (top) and H_2O (bottom). The lines represent the best-matching models.

Concerning the primary adsorption, we always find a dense thin protein layer at the PS surface. For low σ an additional layer, thicker and more dilute, occurs on top of the inner layer (Figure 6). The precision of the determined protein layer

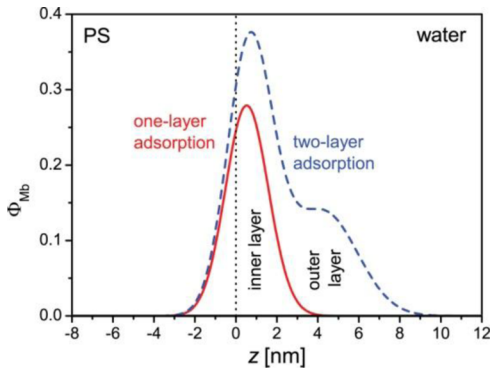

Figure 6. One-layer (solid line) and two-layer (dashed line) primary protein adsorption as obtained by neutron reflectometry for brushes with $N = 770$ at high grafting density and $N = 146$ at low grafting density, respectively (see Table 1).

thicknesses, d_{in} and d_{out}, is limited by the q_z-range of the reflectivity measurements. With this in mind we obtain $d_{in} = 16 \pm 8$ Å for the thickness of the inner protein layer. The thickness of the outer layer, approximated here as the full width at half-maximum (fwhm) of the Gaussian distribution, is $d_{out} = (30 \pm 8)$ Å $\approx 2d_{in}$. Recalling the dimensions of Mb, 45 Å × 35 Å × 25 Å, this suggests that the protein in the inner layer denatures and spreads out upon adsorption, while the protein in the outer layer retains its native state. Comparable results (11 Å $\leq d_{in} \leq$ 26 Å and 31 Å $\leq d_{out} \leq$ 58 Å) were reported for the bare surfaces.[12] Our interpretation suggests that the outer layer formation is due to protein attraction to the proteins adsorbed at the inner layer rather than to ternary adsorption driven by PEG–protein attraction. This view is motivated by two observations: (i) A similar structure was observed on bare PS where ternary adsorption is impossible.[12] (ii) The outer layer is localized in a narrow region in the vicinity of the inner layer in distinction to the behavior expected for ternary adsorption.[23]

C. Influence of Brush Characteristics on Mb Adsorption. The total mass of adsorbed Mb per unit area is specified by

dx.doi.org/10.1021/la403355r | Langmuir 2013, 29, 14178–14187

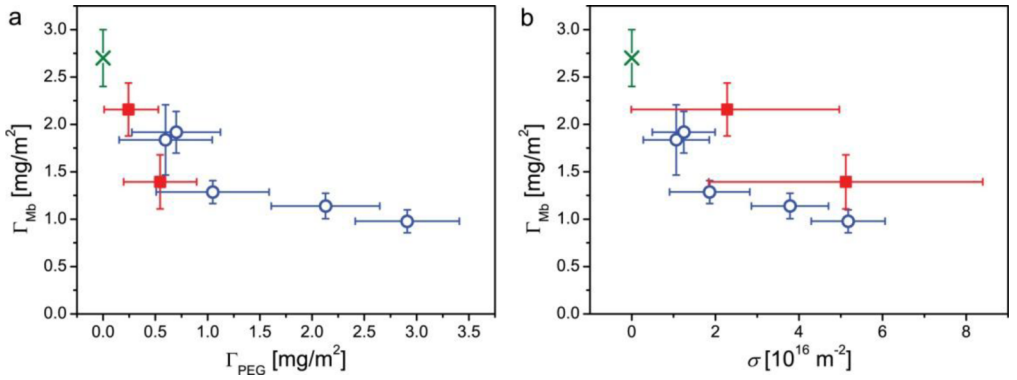

Figure 7. Total adsorbed protein amount Γ_{Mb} as a function of Γ_{PEG} (panel a) and σ (panel b) for brushes with N = 770 (circles) and N = 146 (squares). The X indicates the value obtained by Brouette at al. on bare PS surfaces.[12]

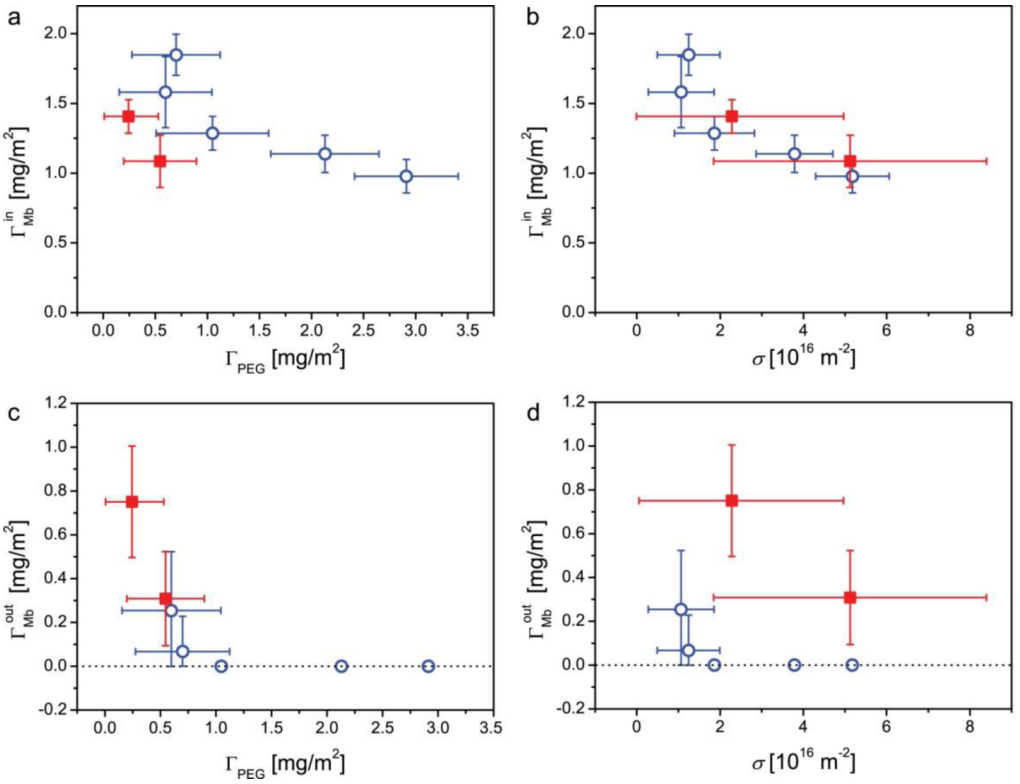

Figure 8. Dependence of inner-layer (panels a and b) and outer-layer (panels c and d) Mb adsorption, Γ^{in}_{Mb} and Γ^{out}_{Mb}, on Γ_{PEG} (panels a and c) and σ (panels b and d). Data points with no error bars correspond to no detected outer layer.

$$\Gamma_{Mb} = \frac{m_{Mb}}{v_{Mb}} \int \Phi_{Mb}(z)\, dz \tag{13}$$

where m_{Mb} and v_{Mb} denote, respectively, the mass and the volume of a Mb molecule and v_{Mb} is set by ρ_{Mb} via $\rho_{Mb} = b_{Mb}/v_{Mb}$, where b_{Mb} is the total scattering length of a Mb molecule. To facilitate comparison with other experimental techniques, we report Γ_{Mb} corresponding to the mass of hydrogenated Mb. As shown in Figure 7, Γ_{Mb} varies with Γ_{PEG} and σ; however the data points for N = 770 and N = 146 in the Γ_{Mb} vs Γ_{PEG} plot tend to collapse onto a single curve. Γ_{Mb} decreases with increasing Γ_{PEG} and σ. For sparsely grafted brushes with low Γ_{PEG} and σ, Γ_{Mb} approaches the value reported[12] for bare hydrophobic surfaces, Γ_{Mb} = (2.7 ± 0.3) mg/m^2. Even at the highest studied grafting densities the Mb adsorption remains significant.

It is instructive to consider separately the Mb adsorption due to the inner and outer layers. These are specified by

$$\Gamma^{in}_{Mb} = \frac{m_{Mb}}{v_{Mb}} \int \Phi^{in}_{Mb}(z)\, dz \tag{14}$$

and

$$\Gamma^{out}_{Mb} = \frac{m_{Mb}}{v_{Mb}} \int \Phi^{out}_{Mb}(z)\, dz \tag{15}$$

see also Table 1. As expected, the plots of Γ^{in}_{Mb} and Γ^{out}_{Mb} vs Γ_{PEG} and σ (Figure 8) are qualitatively similar to the corresponding Γ_{Mb} plots. Note, however, that the Γ^{in}_{Mb} data points for N = 770 and N = 146 collapse onto a single line when plotted vs σ, while Γ^{out}_{Mb} data points are better collapsed when plotted vs Γ_{PEG}.

Our results suggest that the inner layer is sensitive to σ rather than N, while the outer layer is sensitive to both σ and N. These

dx.doi.org/10.1021/la403355r | Langmuir 2013, 29, 14178−14187

conclusions are reminiscent of a theoretical model rationalizing protein adsorption in terms of the osmotic penalty F_{ins} incurred upon inserting the protein into the brush.[8−10] However, the case considered here is likely to involve different physics because a rough estimate suggests $F_{ins} < k_BT$. This estimate invoking the Alexander model[38] in athermal solvent yields an upper bound of the osmotic pressure, $\Pi \approx k_BT/\xi^3$, where $\xi = \sigma^{-1/2}$ is the blob size. $F_{ins} \approx \Pi r_{Mb}^3$ is much smaller than k_BT and thus negligible when $r_{Mb} \ll \sigma^{-1/2}$ [8,10] as is the case for all samples here reported. The tendency of Γ_{Mb}^{in} to decrease with increasing σ may be due to steric screening of the adsorbing PS surface by the terminally grafted PEG chains: The surface required to accommodate a Mb molecule with volume v_{Mb} flattened to a thickness of $d_{in} = 16 \pm 8$ Å is of the order of $v_{Mb}/d_{in} \approx 2000$ Å^2, which is comparable to the area per grafting point in the studied σ range ($\sigma^{-1} \geq 2000$ Å^2). A second adsorbed protein layer as found here for brushes and in a previous study concerning bare PS[12] was not considered in existing theoretical models. These distinguish between primary adsorption at the grafting surface, driven by substrate protein attraction, and ternary adsorption within the brush arising because of monomer protein attractions. The outer protein layer is localized at the exterior boundary of the primary adsorption region and thus may be due to protein−protein attraction. The protein−protein interaction can be reduced by the presence of PEG in the vicinity of the surface and may thus be sensitive to Γ_{PEG}.

D. Exchange of Deuterated and Hydrogenated Proteins. The study of exchange between adsorbed and free proteins is enabled by a number of techniques such as radioactive labeling. NR permits us to follow the exchange and identify the spatial distribution of exchange sites. To this end we first incubated the PEG brush in solution of deuterated Mb and then immersed the brushes in solution of hydrogenated Mb. An exchange between the deuterated and the hydrogenated forms is evidenced by the effect on the reflectivity curves before and after contact with the hydrogenated form. The adsorption is irreversible on the time scale of the experiment when the two reflectivity curves are identical. In our experiment the adsorption of deuterated Mb was carried out as described in the Experimental section, and the exchange was monitored after contacting the brushes for 72 h with an identical solution of hydrogenated Mb. The reflectivity curves did not change significantly within this time scale (see Supporting Information). The Mb exchange experiments thus suggest also that immersion in a neat solvent has negligible effect on measurements involving short immersion in a pure contrast fluid. This last conclusion is consistent with the experimental observation that protein desorption into pure solvents proceeds too slowly to be detected.[5]

IV. CONCLUSIONS

NR with contrast variation allows characterizing the concentration profile of deuterated proteins adsorbed within the brush. It thus enables to distinguish among primary adsorption at the grafting surface, secondary adsorption at the brush outer edge, and ternary adsorption within the brush itself. For the particular systems considered, of Mb adsorbing onto PEG brushes, we find direct evidence for primary adsorption, while significant secondary or ternary adsorption can be excluded. For low grafting densities we identify a modified form of primary adsorption, where denaturated proteins adsorbed at the grafting surface support additional adsorption of proteins in a dilute outer layer in grazing contact with the inner layer. The results suggest that the amount of protein adsorbed in the inner layer correlates to the PEG grafting density, while the amount of protein adsorbed in the outer layer is correlated to the total amount of grafted PEG. We emphasize that traditional techniques such as ellipsometry, radioactive labeling, or quartz crystal microbalance are unable to directly distinguish between these scenarios.

The combination of deuterated proteins with contrast variation enhances the sensitivity of the NR measurements. The usage of this approach requires care in data analysis to allow for exchange of labile hydrogens of the protein with the contrast fluid. As a result the protein SLD varies with the H/D ratio of the contrast fluid. We should add that the concentration profiles of PEG and proteins can be determined with higher precision by using different contrast fluids, namely, brush-matched and protein-matched H_2O/D_2O mixtures. Such studies are currently hampered by the availability of deuterated proteins. Because of the toxicity of deuterium to higher animals, the preparation of deuterated proteins involves their expression in microbial strains that tolerate culture media containing 100% D_2O. The specialized nature of this time-consuming procedure may require a dedicated facility such as the one at the ILL. While our study utilized deuterated Mb, it is important to note the feasibility of NR using nondeuterated proteins in spite of the lower maximal SLD contrast.

■ ASSOCIATED CONTENT

Supporting Information

(1) Reflectivity curves in H_2O contrast of dense $N = 770$ brushes with adsorbed deuterated myoglobin before and after incubation with a solution of hydrogenated myoglobin. (2) A table summarizing the scattering length densities of the contrast fluids as obtained from the reflectivity fits. This material is available free of charge via the Internet at http://pubs.acs.org.

■ AUTHOR INFORMATION

Corresponding Author

*E-mail: fragneto@ill.fr.

Author Contributions

E.S. and A.S. contributed equally to the work.

Notes

The authors declare no competing financial interest.

■ ACKNOWLEDGMENTS

The authors thank ILL for beam time allocation and use of support laboratories for sample preparation and precharacterization within the PSCM initiative. Jean Daillant is thanked for insightful comments. E.S. acknowledges support from a Marie Curie Intra-European Fellowship within the European Commission seventh Framework Program.

■ REFERENCES

(1) Balazs, A. C.; Emrick, T.; Russell, T. P. Nanoparticle Polymer Composites: Where Two Small Worlds Meet. *Science* **2006**, *314*, 1107−1110.

(2) Nishidas, K.; Yamato, M.; Hayashida, Y.; Watanabe, K.; Yamamoto, K.; Adachi, E.; Nagai, S.; Kikuchi, A.; Maeda, N.; Watanabe, H.; Okano, T.; Tano, Y. Corneal Reconstruction with Tissue-Engineered Cell Sheets Composed of Autologous Oral Mucosal Epithelium. *N. Engl. J. Med.* **2004**, *351*, 1187−1196.

(3) Harris, J. M.; Chess, R. Effect of Pegylation on Pharmaceuticals. *Nat. Rev. Drug Discovery* **2003**, *2*, 214−221.

(4) Bockstaller, M. R.; Thomas, E. L. Proximity Effects in Self-Organized Binary Particle-Block Copolymer Blends. *Phys. Rev. Lett.* **2004**, *93*, 166106.
(5) Baszkin, A.; Norde, W. *Physical Chemistry of Biological Interfaces*; Marcel Dekker: New York, 2000.
(6) Currie, E. P. K.; Norde, W.; Cohen Stuart, M. A. Tethered Polymer Chains: Surface Chemistry and Their Impact on Colloidal and Surface Properties. *Adv. Colloid Sci.* **2003**, *100−102*, 205−265.
(7) Currie, E. P. K.; van der Gucht, J.; Borisov, O. V.; Cohen Stuart, M. A. Stuffed Brushes: Theory and Experiment. *Pure Appl. Chem.* **1999**, *71*, 1227−1241.
(8) Halperin, A.; Fragneto, G.; Schollier, A.; Sferrazza, M. Primary Versus Ternary Adsorption of Proteins onto Peg Brushes. *Langmuir* **2007**, *23*, 10603−10617.
(9) Halperin, A.; Kroger, M. Ternary Protein Adsorption onto Brushes: Strong Versus Weak. *Langmuir* **2009**, *25*, 11621−11634.
(10) Halperin, A. Polymer Brushes That Resist Adsorption of Model Proteins: Design Parameters. *Langmuir* **1999**, *15*, 2525−2533.
(11) Szleifer, I. Protein Adsorption on Surfaces with Grafted Polymers: A Theoretical Approach. *Biophys. J.* **1997**, *72*, 595−612.
(12) Brouette, N.; Fragneto, G.; Cousin, F.; Moulin, M.; Haertlein, M.; Sferrazza, M. A Neutron Reflection Study of Adsorbed Deuterated Myoglobin Layers on Hydrophobic Surfaces. *J. Colloid Interface Sci.* **2013**, *390*, 114−120.
(13) Jeon, S. I.; Lee, J. H.; Andrade, J. D.; De Gennes, P. G. Protein-Surface Interactions in the Presence of Polyethylene Oxide: I. Simplified Theory. *J. Colloid Interface Sci.* **1991**, *142*, 149−158.
(14) Harris, J. M. *Poly(Ethylene Glycol) Chemistry: Biotechnical and Biomedical Applications*; Plenum Press: New York, 2003.
(15) Elbert, D. L.; Hubbell, J. A. Surface Treatments of Polymers for Biocompatibility. *Annu. Rev. Mater. Sci.* **1996**, *26*, 365−394.
(16) Goddard, J. M.; Hotchkiss, J. H. Polymer Surface Modification for the Attachment of Bioactive Compounds. *Prog. Polym. Sci.* **2007**, *32*, 698−725.
(17) Cooperstein, M. A.; Canavan, H. E. Biological Cell Detachment from Poly(N-Isopropyl Acrylamide) and Its Applications. *Langmuir* **2010**, *26*, 7695−7707.
(18) Cole, M. A.; Voelcker, N. H.; Thissen, H.; Griesser, H. J. Stimuli-Responsive Interfaces and Systems for the Control of Protein-Surface and Cell-Surface Interactions. *Biomaterials* **2009**, *30*, 1827−1850.
(19) Nagase, K.; Kobayashi, J.; Okano, T. Temperature-Responsive Intelligent Interfaces for Biomolecular Separation and Cell Sheet Engineering. *J. Royal Soc. Interface* **2009**, *6*, S293−S309.
(20) Li, L.; Zhu, Y.; Li, B.; Gao, C. Fabrication of Thermoresponsive Polymer Gradients for Study of Cell Adhesion and Detachment. *Langmuir* **2008**, *24*, 13632−13639.
(21) Takahashi, H.; Nakayama, M.; Yamato, M.; Okano, T. Controlled Chain Length and Graft Density of Thermoresponsive Polymer Brushes for Optimizing Cell Sheet Harvest. *Biomacromolecules* **2010**, *11*, 1991−1999.
(22) Xue, C.; Choi, B.-C.; Choi, S.; Braun, P. V.; Leckband, D. E. Protein Adsorption Modes Determine Reversible Cell Attachment on Poly(N-Isopropyl Acrylamide) Brushes. *Adv. Funct. Mater.* **2012**, *22*, 2394−2401.
(23) Halperin, A.; Kroger, M. Theoretical Considerations on Mechanisms of Harvesting Cells Cultured on Thermoresponsive Polymer Brushes. *Biomaterials* **2012**, *33*, 4975−4987.
(24) Vig, J. R. UV/Ozone Cleaning of Surfaces. *J. Vac. Sci. Technol. A* **1985**, *3*, 1027.
(25) Bosker, W. T. E.; Iakovlev, P. A.; Norde, W.; Cohen Stuart, M. A. Bsa Adsorption on Bimodal Peo Brushes. *J. Colloid Interface Sci.* **2005**, *286*, 496−503.
(26) Norde, W.; Gage, D. Interaction of Bovine Serum Albumin and Human Blood Plasma with Peo-Tethered Surfaces: Influence of Peo Chain Length, Grafting Density, and Temperature. *Langmuir* **2004**, *20*, 4162−4167.
(27) de Vos, W. M.; de Keizer, A.; Kleijn, J. M.; Cohen Stuart, M. A. The Production of Peo Polymer Brushes Via Langmuir-Blodgett and Langmuir-Schaeffer Methods: Incomplete Transfer and Its Consequences. *Langmuir* **2009**, *25*, 4490−4497.
(28) Tamm, L.; McConnell, H. M. Supported Phospholipid Bilayers. *Biophys. J.* **1984**, *47*, 105−113.
(29) Burgess, R. Protein Purification. In *Proteomics of the Nervous System*; Nothwang, H. G., Pfeiffer, S. E., Eds.; Wiley: New York, 2008.
(30) Artero, J.-B.; Haertlein, M.; McSweeney, S.; Timmins, P. A Comparison of Refined X-Ray Structures of Hydrogenated and Perdeuterated Rat Gammae-Crystallin in H_2O and D_2O. *Acta Crystallogr.* **2005**, *61*, 1541−1549.
(31) Hazemann, I.; Dauvergne, M. T.; Blakeley, M. P.; Meilleur, F.; Haertlein, M.; Van Dorsselaer, A.; Mitschler, A.; Myles, D. A. A.; Podjarny, A. High-Resolution Neutron Protein Crystallography with Radically Small Crystal Volumes: Application of Perdeuteration to Human Aldose Reductase. *Acta Crystallogr.* **2005**, *61*, 1413−1417.
(32) Shu, F.; Ramakrishnan, V.; Schoenborn, B. P. Enhanced Visibility of Hydrogen Atoms by Neutron Crystallography on Fully Deuterated Myoglobin. *Proc. Natl. Acad. Sci. U.S.A.* **2000**, *97*, 3872−3877.
(33) Stryer, L. *Biochemistry*; Freeman & Company, W. H.: Cranbury, NJ, 1981.
(34) Wu, H.; Fan, Y.; Sheng, J.; Sui, S.-F. Introduction of Changes in the Secondary Structure of Globular Proteins by a Hydrophobic Surface. *Eur. Biophys. J.* **1993**, *22*, 201−205.
(35) Kondo, A.; Murakami, F.; Higashitani, K. Circular Dichroism Studies on Conformational Changes in Protein Molecules Upon Adsorption on Ultrafine Polystyrene Particles. *Biotechnol. Bioeng.* **1992**, *40*, 889−894.
(36) Cubitt, R.; Fragneto, G. D17: The New Reflectometer at the ILL. *Appl. Phys. A: Mater. Sci. Process.* **2002**, *74*, S329−S331.
(37) Loizou, E.; Porcar, L.; Schexnailder, P.; Schmidt, G.; Butler, P. Shear-Induced Nanometer and Micrometer Structural Responses in Nanocomposite Hydrogels. *Macromolecules* **2010**, *43*, 1041−1049.
(38) Alexander, S. Adsorption of Chain Molecules with a Polar Head a Scaling Description. *J. Phys. (Paris)* **1977**, *38*, 983−987.
(39) Milner, S. T.; Witten, T. A.; Cates, M. E. Theory of the Grafted Polymer Brush. *Macromolecules* **1988**, *21*, 2610−2619.
(40) Milner, S. T. Polymer Brushes. *Science* **1991**, *251*, 905−914.
(41) Zhulina, E. B.; Borisov, O. V.; Priamitsyn, V. A. Theory of Steric Stabilization of Colloid Dispersions by Grafted Polymers. *J. Colloid Interface Sci.* **1990**, *137*, 495−511.
(42) Hill, R. Hydrodynamics and Electrokinetics of Spherical Liposomes with Coatings of Terminally Anchored Poly(Ethylene Glycol): Numerically Exact Electrokinetcs with Self-Consistent Mean-Field Polymer. *Phys. Rev. E* **2004**, *70*, 051406.
(43) Lyngs Hansen, P.; Cohen, J. A.; Podgornik, R.; Parsegian, V. A. Osmotic Properties of Poly(Ethylene Glycols): Quantitative Features of Brush and Bulk Scaling Laws. *Biophys. J.* **2003**, *84*, 350−355.
(44) Rubinstein, M.; Colby, R. H. *Polymer Physics*; Oxford University Press: Oxford, U.K., 2003.
(45) Kawaguchi, S.; Imai, G.; Suzuki, J.; Miyahara, A.; Kitano, T.; Ito, K. Aqueous Solution Properties of Oligo- and Poly(Ethylene Oxide) by Static Light Scattering and Intrinsic Viscosity. *Polymer* **1997**, *38*, 2885−2891.
(46) Brandrup, J.; Immergut, E. H. *Polymer Handbook*; Interscience: New York, 1966.
(47) Ermilov, V.; Lazutin, A.; Halperin, A. Colloids in Brushes: The Insertion Free Energy Via Monte Carlo Simulation with Umbrella Sampling. *Macromolecules* **2010**, *43*, 3511−3520.
(48) Parratt, L. G. Surface Studies of Solids by Total Reflection of X-Rays. *Phys. Rev.* **1954**, *95*, 359−369.
(49) Press, W. H.; Teukolsky, S. A.; Vetterling, W. T.; Flannery, B. P. *Numerical Recipes in C*, 2nd ed.; Cambridge University Press: Cambridge, 1992.
(50) Bevington, P. R.; Robinson, D. K. *Data Reduction and Error Analysis for the Physical Sciences*; McGraw-Hill: New York, 2003.
(51) Hellstrand, E.; Grey, M.; Ainalem, M.-L.; Ankner, J.; Forsyth, V. T.; Fragneto, G.; Haertlein, M.; Dauvergne, M.-T.; Nilsson, H.; Brundin, P.; Linse, S.; Nylander, T.; Sparr, E. Adsorption of A-

Synuclein to Supported Lipid Bilayers: Positioning and Role of Electrostatics. *ACS Chem. Neurosci.* **2013**, *4*, 1339−1351.
(52) Fragneto, G.; Lu, J. R.; McDermott, D. C.; Thomas, R. K.; Rennie, A. R.; Gallagher, P. D.; Satija, S. K. Structure of Monolayers of Tetraethylene Glycol Monodecyl Ether Adsorbed on Self-Assembled Monolayers on Silicon: A Neutron Reflectivity Study. *Langmuir* **1996**, *12*, 477−486.
(53) Fragneto, G.; Thomas, R. K.; Rennie, A. R.; Penfold, J. Neutron Reflection Study of Bovine Beta-Casein Adsorbed on OTS Self-Assembled Monolayers. *Science* **1995**, *267*, 657−660.
(54) McDermott, D. C.; Lu, J. R.; Lee, E. M.; Thomas, R. K.; Rennie, A. R. Study of the Adsorption from Aqueous Solution of Hexaethylene Glycol Monodecyl Ether on Silica Substrates Using the Technique of Neutron Reflection. *Langmuir* **1992**, *8*, 1204−1210.
(55) Lu, J. R.; Su, T. J.; Thirtle, P. N.; Thomas, R. K.; Rennie, A. R.; Cubitt, R. The Denaturation of Lysozyme Layers Adsorbed at the Hydrophobic Solid/Liquid Surface Studied by Neutron Reflection. *J. Colloid Interface Sci.* **1998**, *206*, 212−223.